

Article

Adsorption of Ammonium Nitrogen from Aqueous Solution on Chemically Activated Biochar Prepared from Sorghum Distillers Grain

Derlin Hsu ¹, **Changyi Lu** ¹, **Tairan Pang** ², **Yuanpeng Wang** ³ and **Guanhua Wang** ^{2,*}¹ College of the Environment and Ecology, Xiamen University, Xiamen 361005, China; terlinhsu@gmail.com (D.H.); lucy@xmu.edu.cn (C.L.)² Tianjin Key Laboratory of Pulp and Paper, College of Light Industry Science and Engineering, Tianjin University of Science and Technology, Tianjin 300457, China; pangtr1995@163.com³ Department of Chemical and Biochemical Engineering, College of Chemistry and Chemical Engineering, Xiamen University, Xiamen 361005, China; wypp@xmu.edu.cn

* Correspondence: ghwang@tust.edu.cn; Tel.: +86-022-60601313

Received: 3 November 2019; Accepted: 28 November 2019; Published: 3 December 2019



Abstract: Chemically activated biochars prepared from sorghum distillers grain using two base activators (NaOH and KOH) were investigated for their adsorption properties with respect to ammonium nitrogen from aqueous solution. Detailed characterizations, including scanning electron microscopy (SEM), Fourier transform infrared spectroscopy (FTIR), X-ray diffraction (XRD), thermogravimetry (TG), and specific surface area analyses, were carried out to offer a broad evaluation of the prepared biochars. The results showed that the NaOH- and KOH-activated biochars exhibited significantly enhanced adsorption capacity, by 2.93 and 4.74 times, respectively, in comparison with the pristine biochar. Although the NaOH-activated biochar possessed larger specific surface area (132.8 and 117.7 m²/g for the NaOH- and KOH-activated biochars, respectively), the KOH-activated biochar had higher adsorption capacity owing to its much higher content of functional groups. The adsorption kinetics and isotherms of the KOH-activated biochar at different temperatures were further studied. The biochar had a maximum adsorption capacity of 14.34 mg/g at 45 °C, which was satisfactory compared with other biochars prepared using different feedstocks. The adsorption process followed pseudo-second-order kinetics, and chemical adsorption was the rate-controlling step. The equilibrium data were consistent with the Freundlich isotherm, and the thermodynamic parameters suggested that the adsorption process was endothermic and spontaneous. Consequently, this work demonstrates that chemically activated biochar from sorghum distillers grain is effective for ammonium nitrogen removal.

Keywords: sorghum distillers grain; biochar; chemical activation; ammonium nitrogen adsorption; adsorption kinetics and isotherms

1. Introduction

Water pollution has become a major concern, and water pollution control has been regarded as a priority for both society and public authorities [1]. The chemical compositions of natural water resources are primarily determined by industrial, domestic, and agricultural practices, geology, climate, and other natural and anthropic sources [2]. The anthropogenic pollutants, such as nitrogen compounds, metals, pesticides, pharmaceuticals, personal care products, etc., have a critical effect on the quality of water resources [3]. Among them, ammonium nitrogen is a common water contaminant and is generally released into the environment through industrial effluent and agricultural drainage [4]. Excess ammonium nitrogen in water leads to a series of ecological problems in aquatic environments

related to eutrophication, including acidification of freshwater ecosystems, hypoxic water conditions, and toxicity to benthic organisms and fish [5]. Moreover, ammonium nitrogen can result in the generation of genotoxic nitrosodimethylamine [6]. Therefore, for public health and environmental safety, the removal of ammonium nitrogen from contaminated water is urgently required.

Different technologies have been developed to remove ammonium nitrogen from wastewater, including biological treatments [7], ion exchange [8], adsorption [9], electrodialysis [10], and reverse osmosis [11]. Among these technologies, adsorption has gained extensive attention owing to its obvious advantages, such as high efficiency and a simple process [12,13]. Another advantage of adsorption for ammonium nitrogen removal is that a wide range of adsorbents is available. Reported adsorbents for ammonium nitrogen removal include agricultural by-products [9], zeolite [6], resin [14], and hydrogel composites [15]. Currently, there is growing interest in developing effective adsorbents from low-cost renewable biomass resources, owing to their sustainability and economic efficiency.

Biochar is a carbon-rich solid prepared from biomass pyrolysis, especially low-cost biomass, under oxygen-limited condition. Owing to its favorable characteristics, including high porosity and cation exchange capacity, biochar shows good adsorption performance towards many pollutants from industrial, agricultural, and domestic waste waters [16]. Therefore, biochars prepared from different sources, such as plant biomass, corn cob, and giant reed, have been studied as effective and low-cost adsorbents for ammonium nitrogen [9,12,17]. More importantly, biochar after the adsorption of ammonium nitrogen can be further employed as slow-release fertilizer, which realizes the reutilization of the used adsorbent [17,18].

Sorghum distillers grain (SDG) is a solid waste from white spirits industry using sorghum as the raw material. Sorghum is a drought-tolerant plant that can easily adapt to arid climates. Due to its easy cultivation and high productivity, sorghum is widely used for liquor production. SDG contains starch, cellulose, protein, and lipid, and has been utilized as animal feed [19]. However, SDG is difficult to store since it rots rapidly because of its high moisture content and fermentable sugar content. Using distillers grain to prepare biochar by pyrolysis has been proposed as an alternative method since these fermentation residues have the potential to be converted into carbonaceous material. Although biochar prepared from brewers' spent grain [17], also a fermentation residue, has been reported as an adsorbent for ammonium nitrogen capture, there is a lack of studies on the physicochemical properties and ammonium nitrogen adsorption performance of biochar produced from SDG. It is well known that the feedstock source has a critical impact on the properties of the prepared biochar, including the specific surface area and content of surface functional groups [12,20]. In addition, chemical activation is considered an efficient method to improve the biochar adsorption capacity [21,22], and reports regarding the use of activators in biochar preparation from SDG are scarce. Therefore, the current study focuses on the physicochemical characterization of chemically activated biochar produced from SDG and the evaluation of its adsorption capacity for ammonium nitrogen.

In this work, biochars derived from SDG through NaOH- and KOH-activated pyrolysis processes were studied for the adsorption of ammonium nitrogen from a simulated aqueous solution. Detailed characterizations, including scanning electron microscopy (SEM), Fourier transform infrared spectroscopy (FTIR), X-ray diffraction (XRD), thermogravimetry (TG), and specific surface area (SAA) analyses, were carried out to offer a broad evaluation of the prepared biochars. The effects of activators, pyrolysis temperature, and adsorption pH on the biochar adsorption capacity were analyzed. Moreover, the adsorption process was further analyzed based on the adsorption kinetics and isotherm, with the aim to discover the possible adsorption mechanism of ammonium nitrogen on the biochar.

2. Materials and Methods

2.1. Materials and Chemicals

Sorghum distillers grain (SDG) was collected from a sorghum distillery in Kinmen, Taiwan province, China. The sample was dried at 65 °C for 12 h in an oven (VOS-30A, STIK, Shanghai, China) and was ground to a 60–80 mesh particle size using a high-speed multifunction crusher (800, Yongkang Tianqi Shengshi Industry and Trade Co., Ltd., Jinhua, China). KOH, NaOH, 3,5-dinitrosalicylic acid, and petroleum ether were of analytical grade and were purchased from Sinopharm Chemical Reagent Co., Ltd. (Shanghai, China). NH₄Cl was a guaranteed reagent obtained from Macklin Co., Ltd. (Shanghai, China). Biological reagents, including cellulase and amylase, were purchased from Sigma-Aldrich.

2.2. Preparation of Biochar

Three grams of SDG were impregnated in 10 mL 30 g/L NaOH (or KOH) solution for 12 h and oven-dried at 105 °C overnight. Afterward, the SDG samples were ground and placed in a tube furnace (SK2-1-12, Tianye, China) for pyrolysis. The pyrolysis experiments were performed at different temperatures (550, 650, and 750 °C) with a heating rate of 5 °C /min in a sweeping nitrogen gas atmosphere for 2 h, according to the previous study [21]. After pyrolysis, the obtained biochar was washed with excess deionized water three times. The washed biochar was then oven-dried at 105 °C for approximately 5 h and weighed for a yield calculation. For comparison, dried SDG without chemical activation was also pyrolyzed at 650 °C for 2 h with a heating rate of 5 °C /min to obtain an activator-free biochar.

2.3. Ammonium Nitrogen Adsorption Experiments

To evaluate the ammonium nitrogen adsorption performance of the biochar samples, a series of adsorption experiments were conducted using a 100 mL conical flask containing 25 mL NH₄Cl aqueous solution. Typically, 0.1 g biochar was added to 25 mL 100 mg/L NH₄Cl aqueous solution, and the mixture was placed in an electrically thermostatic shaker (HNY-100B, Tianjin Honour Instrument Co., Ltd, Tianjin, China) at 200 rpm at 30 °C for 6 h. The pH of the NH₄Cl aqueous solution was adjusted in the range from 3 to 10 by adding NaOH and HCl. After adsorption, the residual ammonium solution was filtered through a 0.45 µm membrane, and the ammonium concentration in the solution was analyzed using the Nesslerization method with the help of a UV-vis spectrophotometer (Shimadzu UV-2500, Japan) at 420 nm [23]. The ammonium adsorption capacity was calculated based on the following equation:

$$Q_t = (C_0 - C_t)V/m \quad (1)$$

where C_0 is the initial ammonium nitrogen concentration (mg/L), C_t is the residual ammonium nitrogen concentration (mg/L) after biochar adsorption at time t , V (mL) is the solution volume for the adsorption experiment, and m (g) is the adsorbent mass used in the adsorption experiment.

For the adsorption kinetic study, ammonium concentrations at different time points (e.g., 0.5, 1, 1.5, 2, 3, 4, 5, and 6 h) were determined. For the adsorption isotherms, 0.1 g biochar was added to 25 mL NH₄Cl aqueous solution with different concentrations (50, 100, 200, 400, and 600 mg/L). All the adsorption tests were performed in triplicate.

2.4. Composition Analyses of Sorghum Distillers Grain

The ash content was determined by placing the dried SDG samples in a muffle furnace at 600 °C for 2 h. The crude lipid content in the SDG was analyzed by Soxhlet extraction with petroleum ether for 5 h [24]. The solvent was then removed by evaporation under vacuum at 40 °C. The crude protein was determined using the Kjeldahl procedures as described in Association of Official Agricultural Chemists (AOAC, Washington, DC, USA, 1995, 16th ed.) guidelines. The cellulose and starch contents in the SDG were measured by enzymatic methods using cellulase (Sigma-Aldrich) and amylase

(Sigma-Aldrich), respectively. The glucose released after enzymatic saccharification was estimated spectrophotometrically by the 3,5-dinitrosalicylic acid (DNS) method [25]. The element contents (carbon, hydrogen, and nitrogen) in the SDG were obtained using an elemental analyzer (Vario EL III, Elementar, Germany).

2.5. Characterization of Biochar

XRD patterns were obtained from an Ultima IV X-ray diffractometer (Rigaku, Japan), which was operated at 35 kV and a scanning speed of 20°/min in the 2θ range from 10 to 70° using Cu Ka radiation ($k = 1.5418 \text{ \AA}$). FTIR spectra were obtained using a Nicolet Avatar (Thermo Electron, San Jose, CA, USA) and the potassium bromide technique, in a proportion of 1:100 (100 mg of KBr approximately). For zeta potential determination, the biochar sample (0.01 g) was firstly ground to pass through a 200 mesh sieve and well dispersed in 100 mL distilled water (at pH ranging from 3.0 to 10.0, adjusted using NaOH or HCl) by 10 min ultrasonic treatment. The zeta potential was analyzed in triplicate with the help of a Zetasizer Nano ZS instrument (Malvern Instruments Ltd., Worcestershire, UK). The thermal stability of the biochar samples was measured by employing a TG instrument (TA SDT 650, New Castle, DE, USA) with a heating rate of 10 °C/min from 25 to 800 °C under the protection of N₂. The specific surface area of the biochar samples was analyzed using an Automated Physisorption and Chemisorption Analyzer (Tristar 3000, Norcross, GA, USA). The samples were degassed under vacuum at 300 °C for over 3 h before measurements. The morphology of the biochar was observed using a SEM instrument (JSM-5600LV, JEOL Ltd., Tokyo, Japan) operated at a voltage of 20 kV. Boehm titrations of the biochars were conducted according to the protocol described previously [26].

3. Results and Discussion

3.1. Characterization of Sorghum Distillers Grain

The compositions of raw materials have an important effect on the properties of the obtained biochar. Composition analyses of the SDG sample showed that it contained 24.6% ± 0.7% starch, 19.6% ± 0.4% cellulose, 14.9% ± 0.5% protein, 4.4% ± 0.2% crude lipid, and 6.4% ± 0.3% ash. Although the SDG was the residue of sorghum after fermentation, it still had a high content of starch, which was mainly caused by the relatively low hydrolysis efficiency by microbes during fermentation [19,27]. The high contents of cellulose and ash mainly come from the rice husk, which is added to loosen the solid sorghum medium and improve the heat transfer for fermentation and distillation [19]. The elemental analysis suggested that the SDG mainly contained C (44.1%), H (6.5%), and N (2.9%) because of its high starch, cellulose, and protein contents. Accordingly, the presence of high carbon element content makes the SDG a potential feedstock for biochar production.

3.2. Adsorption of Ammonium Nitrogen on Biochar

3.2.1. Effect of activation agents on the adsorption capacity of biochar

Figure 1a shows the NH₄⁺-N adsorption capacity and yields of biochar prepared using NaOH and KOH as activators, as well as those of biochar prepared without chemical activation. The NH₄⁺-N adsorption capacity of the biochar without activation was about 2.06 mg/g, which was in agreement with the result reported by Gai et al. when they analyzed the ammonium nitrogen adsorption capacity of biochar obtained from corn straw [28]. After activation by NaOH and KOH, the biochar samples exhibited significantly enhanced adsorption capacity of 6.03 and 9.77 mg/g, respectively, indicating that the chemical activation facilitated ammonium nitrogen adsorption. The biochar without activation showed obviously higher yield than the two chemically activated biochars. This result can be attributed to the intensified pyrolysis reactions caused by the base catalysts, which convert the solid carbon substances into gaseous carbon volatiles [29]. Although the two activated biochars had similar yields (31.29% and 30.47%), the adsorption capacity of KOH-activated biochar was higher than that of

NaOH-activated biochar. Thus, KOH-activated biochar was chosen as the adsorbent for the following adsorption experiments.

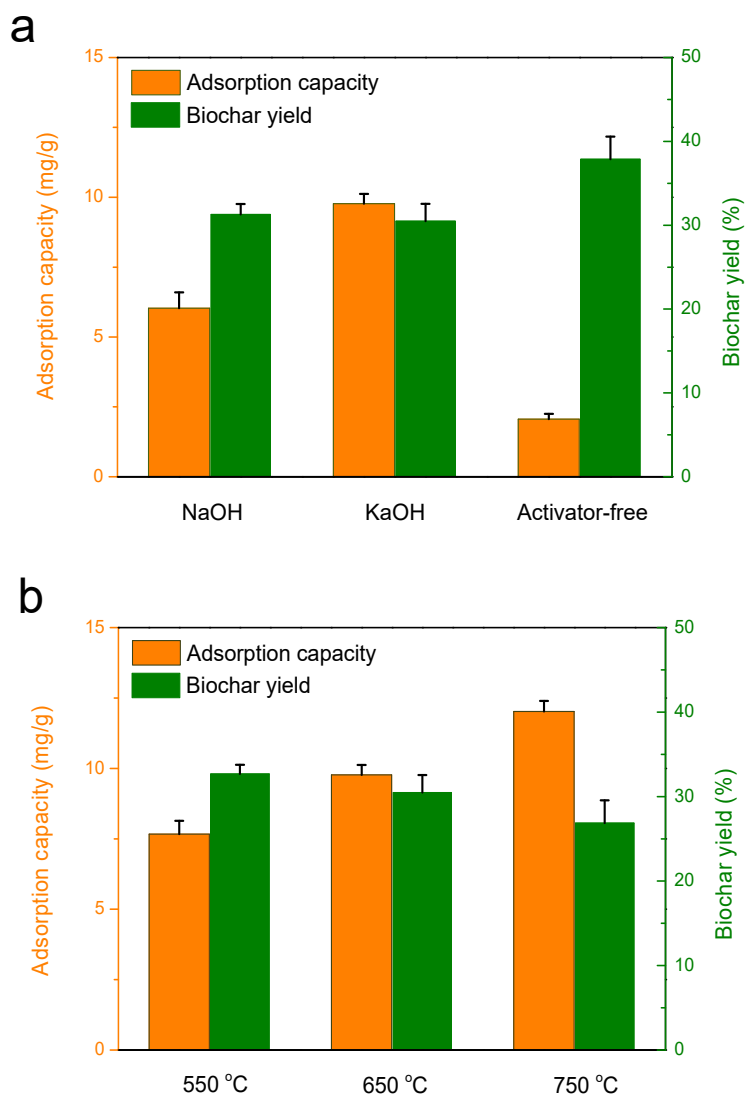


Figure 1. Effect of activators on the yield and NH_4^+ -N adsorption of biochar from sorghum distillers grain (a); Effect of pyrolysis temperature on the yield and NH_4^+ -N adsorption of KOH-activated biochar from sorghum distillers grain (b).

3.2.2. Effect of Activation Temperature on the Adsorption Capacity of Biochar

Figure 1b shows the yield and NH_4^+ -N adsorption capacity of KOH-activated biochar obtained at different pyrolysis temperatures. It was found that increasing the pyrolysis temperature resulted in a decline in biochar yield, which could be explained by the release of more volatile matter during the pyrolysis at a higher temperature [28]. However, the NH_4^+ -N adsorption capacity of the biochar improved when the pyrolysis temperature was increased. The biochar obtained at 550 °C exhibited an adsorption capacity of about 7.67 mg/g, while the value increased significantly to 12.02 mg/g when the pyrolysis temperature was increased to 750 °C. Thus, the NH_4^+ -N capacity of KOH-activated biochar is influenced by the pyrolysis temperature. The pyrolysis temperature has a critical effect on the specific surface area of the prepared biochar and, accordingly, the adsorption capacity of the biochar [28]. The specific surface areas of the KOH-activated biochar pyrolyzed at 550, 650, and 750 °C were 95.9, 117.7, and 155.3 m^2/g , respectively. This result is consistent with those of other studies reporting a high surface area in biochar pyrolyzed at 650–800 °C [30,31]. The low surface area of biochar pyrolyzed at

a lower temperature is caused by the formation of tars, which prevents pore formation during the pyrolysis process. However, when pyrolysis is conducted at a higher temperature, pores are generated easily due to the volatilization of tar components [30].

3.2.3. Effect of Adsorption pH on the Adsorption Capacity of Biochar

The pH value of NH_4^+ -N solution has a critical effect on the charge distribution of biochar and the electrostatic or molecular interactions between the biochar and NH_4^+ -N, which accordingly determine the NH_4^+ -N adsorption capacity of biochar. The effect of adsorption pH on the adsorption capacity of KOH-activated biochar is presented in Figure 2. It was found that the adsorption capacity increased with increasing pH value from 3.0 to 9.0, and further enhancement of the pH resulted in a sharp decrease in adsorption capacity. Similar results have been documented by other researchers [32,33]. The low adsorption capacity at low pH may be caused by the low negative zeta potential of biochar at low pH as shown in Figure 2. Since ammonium nitrogen is a positive ion, biochar with a high negative zeta potential facilitates adsorption through electrostatic attraction. However, when the solution pH value is increased to 10.0, most of the NH_4^+ ion can be transformed into the $\text{NH}_3(\text{aq})$ form as the NH_4^+ ion has a pK_a of about 9.3 [33]. Therefore, at this pH value (10.0), the electrostatic attraction mechanism was no longer effective, which resulted in the observed reduction in the adsorption capacity [32]. It is notable that the pH value of biochar in water without adjustment was about 8.4 and the adsorption capacity of biochar at this pH was almost the same as the highest value at pH 9.0. In order to simplify the adsorption process, the following adsorption experiments were conducted without pH adjustment (pH about 8.4).

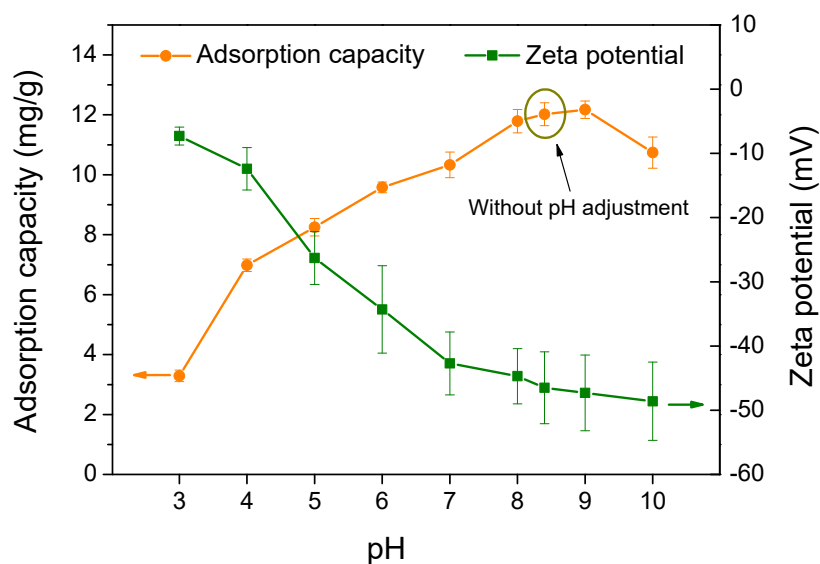


Figure 2. Effect of solution pH on NH_4^+ -N adsorption and the zeta potential of biochar (adsorption conditions: NH_4^+ -N, 100 mg/L; biochar dosage, 4 g/L; temperature, 25 °C).

3.2.4. Adsorption Kinetics

The adsorption kinetics of KOH-activated biochar (produced at 750 °C) at various adsorption temperatures are presented in Figure 3a. It was found that the adsorption trends for different temperature were similar. Specially, the first 2 h were attributed to the rapid adsorption stage for NH_4^+ -N, which was owing to the exposed surface, porous network structure, and the high amounts of vacant adsorption sites. The adsorption capacity (Q_t) increased from 11.58 to 14.34 mg/g when the adsorption temperature increased from 25 to 45 °C. Wang et al. [34] investigated the adsorption of NH_4^+ -N onto progressively oxidized maple wood biochar and found that the maximum adsorption capacity was 10.1 mg/g. Zheng et al. [20] prepared biochar from anaerobic digestion residue, with an

NH_4^+ adsorption capacity of 8.37 mg/g. Zhu et al. [22] prepared activated carbon from avocado seeds through methanesulfonic acid activation and found that its NH_4^+ -N adsorption capacity was 5.4 mg/g.

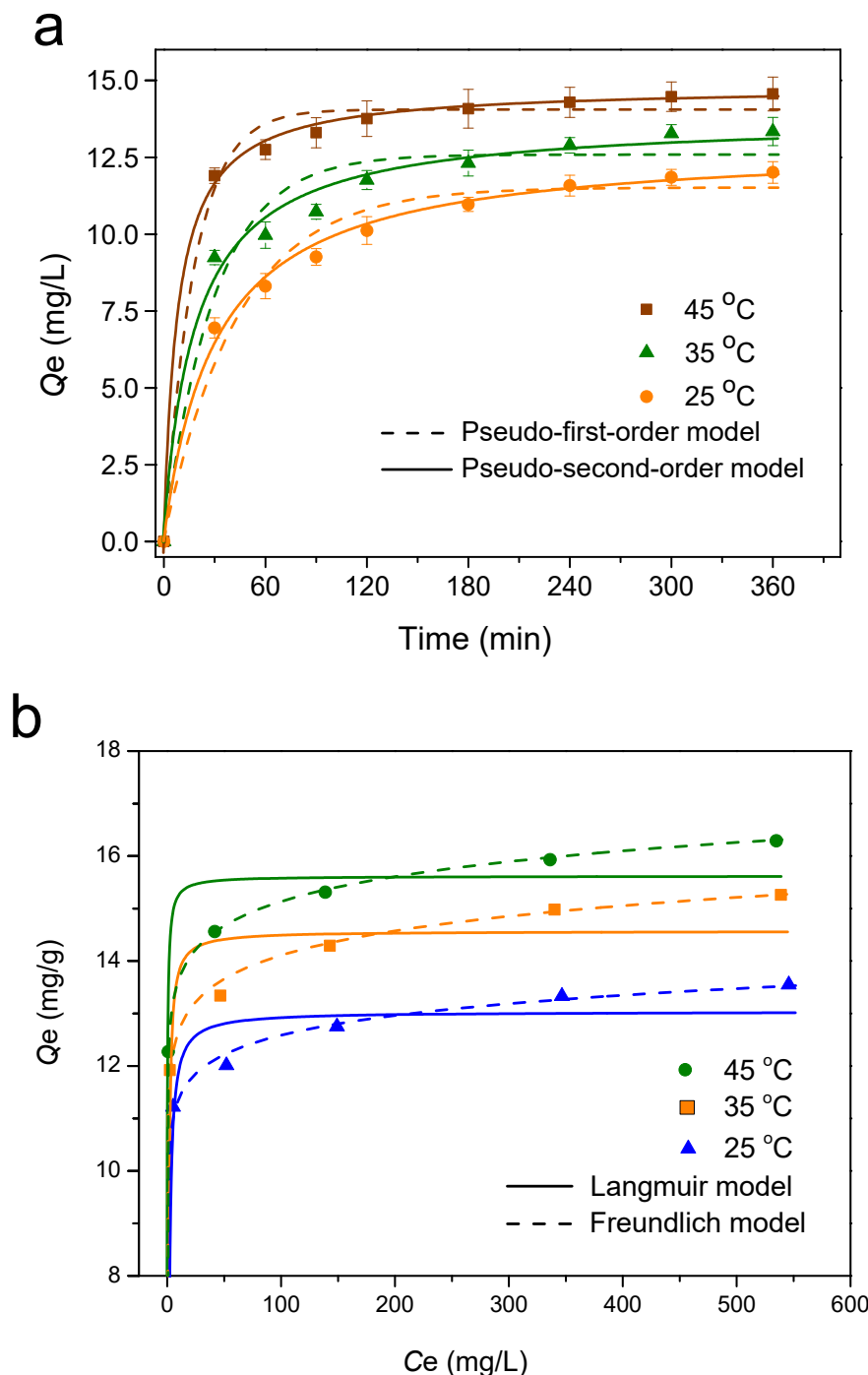


Figure 3. (a) Adsorption kinetics of NH_4^+ -N onto biochar (NH_4^+ -N: 100 mg/L, biochar dosage: 4 g/L, temperature: 25–45 °C), as well as the fitting curves using pseudo-first-order and pseudo-second-order models. (b) Langmuir and Freundlich equilibrium adsorption isotherms for the adsorption of NH_4^+ -N onto biochar (adsorbent dose: 4 g/L, temperature: 25–45 °C).

The adsorption process was further fitted using the pseudo-first-order and pseudo-second-order models, which are expressed in Equations (2) and (3), respectively:

$$Q_t = Q_e(1 - \exp - k_1 t) \quad (2)$$

$$Q_t = \frac{k_2 Q_e^2 t}{1 + k_2 Q_e t} \quad (3)$$

where Q_e (mg/g) is the equilibrium amount of NH_4^+ -N adsorbed by the biochar, Q_t (mg/g) is the amount of NH_4^+ -N adsorbed by the biochar at time t (min), and k_1 (1/min) and k_2 (g/(mg·min)) are the rate constants of the pseudo-first-order model and the pseudo-second-order model, respectively.

The plots of Q_t against t are presented in Figure 3a, and their fitting curves using the two models are also given in Figure 3a. Table 1 shows the results of the nonlinear regression analysis of the two kinetic models. The results in Figure 3a show that the theoretical adsorption capacities ($Q_{e,\text{cal}}$) using the pseudo-second-order kinetic model were closer to the experimental adsorption capacities (Q_e) than those using the pseudo-first-order kinetic model. The pseudo-second-order kinetics model had higher correlation coefficient values (R^2) than the pseudo-first-order model (Table 1). These results suggest that the adsorption of the NH_4^+ -N on KOH-activated biochar followed a pseudo-second-order kinetics model. Besides this, the values of both $Q_{e,\text{cal}}$ and k_2 increased when the temperature was raised from 25 °C to 45 °C, suggesting that the adsorption process was intensified by elevating the adsorption temperature.

Table 1. Parameters of pseudo-first-order and pseudo-second-order kinetics, as well as the experimental and calculated Q_e at different temperatures.

T (°C)	Q_e (mg/g)	Pseudo-First-Order Kinetics			Pseudo-Second-Order Kinetics		
		k_1 (1/min)	$Q_{e,\text{cal}}$ (mg/g)	R^2	k_2 (g/(mg·min))	$Q_{e,\text{cal}}$ (mg/g)	R^2
25	12.01	0.0232	11.44	0.9688	0.0026	12.86	0.9942
35	13.34	0.0338	12.54	0.9543	0.0040	13.72	0.9875
45	14.56	0.0580	14.01	0.9876	0.0086	14.72	0.9985

The relationship between temperature and the rate constant can be described by the Arrhenius equation, which is expressed as follows:

$$\ln k_2 = \ln A - \frac{E_a}{RT} \quad (4)$$

where k_2 (g·mg⁻¹·min⁻¹) is the adsorption rate constant of the pseudo-second-order model, A (min⁻¹) is the pre-exponential factor, and R (8.314 J/(K·mol)) and T (K) are the ideal gas constant and the absolute temperature, respectively. The activation energy (E_a) magnitude can provide an insight into the adsorption type [35]. In this work, the value of E_a for the adsorption of NH_4^+ -N on KOH-activated biochar was 47.01 kJ/mol after calculation, indicating that the adsorption is a chemical adsorption dominant type owing to the high E_a value (>40 kJ/mol).

3.2.5. Adsorption Isotherm

In order to understand how NH_4^+ -N is adsorbed onto the biochar adsorbent, as well as to define the equilibrium data, the adsorbed amounts and residual NH_4^+ -N concentration in the solution after adsorption were fitted using both Langmuir and Freundlich isotherms. The Langmuir model (Equation (5)) indicates monolayer adsorption on a homogenous surface, while the Freundlich isotherm (Equation (6)) elucidates nonideal adsorption on heterogeneous surfaces and multilayer adsorption [36,37]:

$$Q_e = \frac{Q_m k_L C_e}{1 + k_L C_e} \quad (5)$$

$$Q_e = k_F C_e^{\frac{1}{n}} \quad (6)$$

where Q_e is the amount of NH_4^+ -N absorbed (mg/g) and C_e is the equilibrium concentration (mg/L) of NH_4^+ -N in aqueous solution after adsorption. k_L (L/mg) and Q_m (mg/g) are the Langmuir

constant and the monolayer maximum adsorption capacity of NH_4^+ -N onto biochar, respectively. The Freundlich constants k_F and n are the multilayer adsorption capacity (mg/g) and the adsorption intensity, respectively.

The plots of the adsorbed NH_4^+ -N amounts on biochar versus the residual NH_4^+ -N concentration in the solution at different temperatures are given in Figure 3b, as well as the fitting curves using the two isotherm models. The fitting parameters of the biochar adsorption equilibrium data using the two models are shown in Table 2. As shown in Figure 3b, the adsorption process was represented by the Freundlich model very well, and the correlation coefficient (R^2) values were all higher than 0.99 (Table 2). The values of $1/n$ in the Freundlich model were lower than 0.1, suggesting that the adsorption process is favorable [35,38]. The value of $1/n$ can be further divided into five levels, and when the value is between 0.1 and 0.01, the adsorption is categorized as a strongly favorable level, indicating the good adsorption performance of NH_4^+ -N on biochar [39].

Table 2. Adsorption isotherms of ammonium nitrogen onto biochar using Langmuir and Freundlich models.

T (°C)	Langmuir Model			Freundlich Model			Van 't Hoff		
	k_L (L/mg)	Q_m (mg/g)	R^2	n	k_F (mg/g)	R^2	ΔG^0 (kJ/mol)	ΔS^0 (J/(K·mol))	ΔH^0 (kJ/mol)
25	1.143	13.0	0.9899	23.8	10.4	0.9993	-13.82		
35	1.891	14.5	0.9862	21.5	11.4	0.9994	-13.59	589.36	40.47
45	4.000	15.6	0.9900	22.6	12.3	0.9999	-15.00		

Thermodynamic parameters, including Gibbs free energy ΔG^0 (kJ/mol), entropy ΔS^0 (J/(K·mol)), and standard enthalpy ΔH^0 (kJ/mol), can be used to estimate the temperature effect on NH_4^+ -N adsorption onto the biochar and give an idea about the adsorption behavior and mechanism. The thermodynamic parameters can be obtained from the Freundlich model using the following equations [40]:

$$\Delta G = -RT \ln k_d \quad (7)$$

$$\ln k_d = -\frac{\Delta H^0}{RT} + \frac{\Delta S^0}{R} \quad (8)$$

$$k_d = k_F^n \quad (9)$$

where R is the gas constant, the value of which is 8.314 J/(K·mol); T (K) is the absolute temperature; and n and k_F ($\mu\text{mol/g}$) are Freundlich constants. The slope and intercept of the plots of $\ln k_d$ versus $1/T$ are used to calculate the values of ΔH^0 and ΔS^0 .

Table 2 also presents the thermodynamic parameters calculated from Equations (7)–(9). The negative values of ΔG^0 demonstrated the spontaneous nature and the feasibility of the adsorption of NH_4^+ -N on KOH-activated biochar. In addition, the ΔG^0 values became more negative with increasing adsorption temperature, confirming that adsorption is more favorable at higher temperature [35,41]. Meanwhile, the positive value of ΔS^0 indicated the affinity of the biochar for NH_4^+ -N. The positive ΔH^0 reflected the endothermic adsorption of NH_4^+ -N onto biochar [42], which is in agreement with the kinetics results (Section 3.2.3) that increased temperature favors the adsorption.

3.3. Characterization of the Biochar

3.3.1. Scanning Electron Microscopy (SEM)

The morphology of the biochars activated by KOH and NaOH at 650 °C was characterized by SEM, and the results are representatively presented in Figure 4 with different magnifications. It was observed that both of the two biochars had an obvious porous structure, confirming the pore-forming effect of the two activators. The porous structures of the two biochars from the SEM results were also in good agreement with their high SAA values (132.8 and 117.7 m^2/g for NaOH- and KOH-activated biochars,

respectively). The nitrogen adsorption–desorption isotherms of the NaOH- and KOH-activated biochars are presented in Figure 5. It was found that the isotherms belonged to type IV (IUPAC classification), indicating that the two biochars had mesoporous structure [43,44]. When the P/P_0 was higher than 0.95, the increase in the adsorption–desorption isotherms of NaOH-activated biochar was more obvious compared with that of KOH-activated biochar, indicating more macropores in the NaOH-activated biochar [45]. From a higher-magnification observation (Figure 4c,f), NaOH-activated biochar had a thin and fractured pore wall structure, while KOH-activated biochar exhibited a continuous porous structure with relatively thick pore walls. Since the two biochar types were obtained under the same temperature, the obvious difference in porous structures between them was mainly attributed to the different activation effects of the two activators [29]. Besides this, there was no significant difference in the porous structures of the two biochars after $\text{NH}_4^+ \text{-N}$ adsorption, suggesting good mechanical properties of the prepared biochars [12].

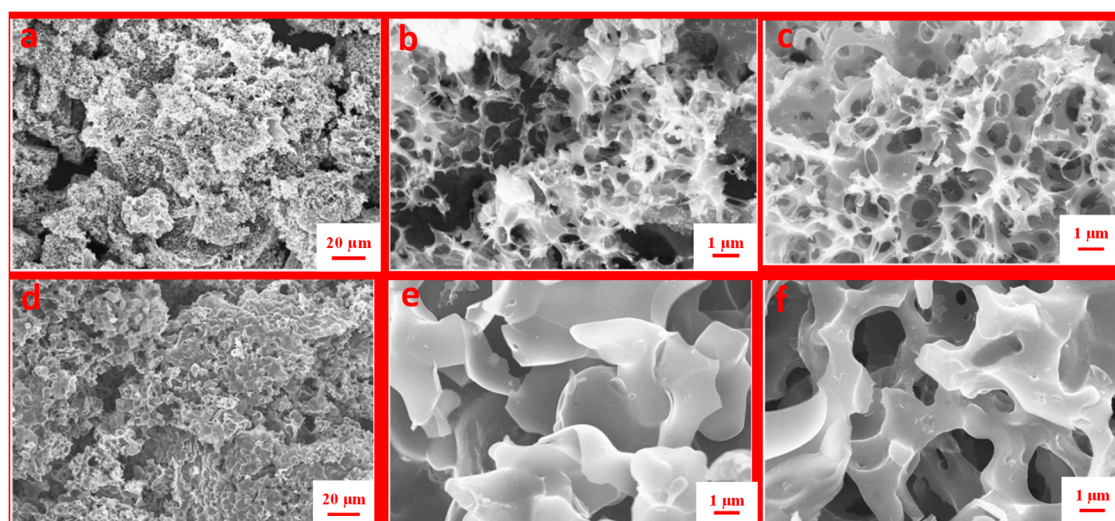


Figure 4. SEM images of NaOH-activated biochar (a,b) and KOH-activated biochar (d,e), (c,f) represent the NOH-activated biochar and KOH-activated biochar, respectively, after ammonium nitrogen adsorption.

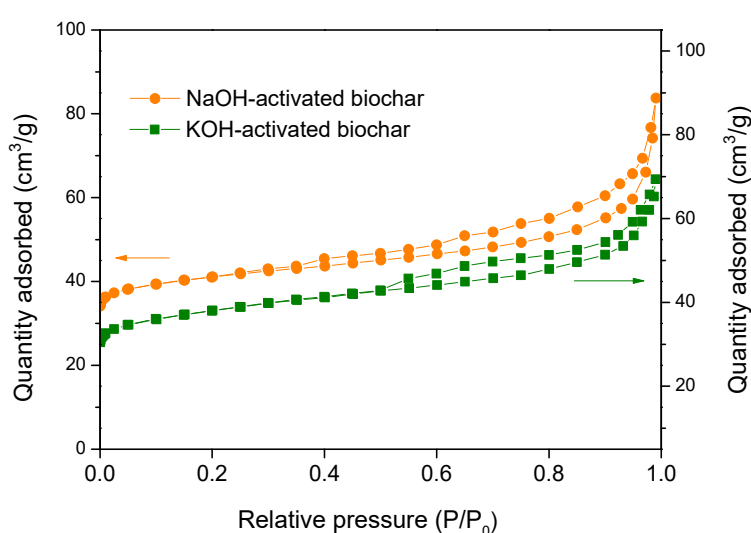


Figure 5. Nitrogen adsorption–desorption isotherms of NaOH-activated biochar and KOH-activated biochar.

3.3.2. X-Ray Diffraction (XRD)

The XRD patterns of the NaOH-activated biochar and KOH-activated biochar before and after NH_4^+ -N adsorption are shown in Figure 6. All the four biochar samples exhibited analogous diffractogram patterns with a broad peak in the range of 20–30°. The broad peak was attributed to the characteristics of amorphous carbon, which was disorderly stacked up by carbon rings [46]. However, two sharp peaks at 28° and 41° assigned to sylvite (KCl) were found from the XRD pattern of KOH-activated biochar [12,47]. The sylvite formed in the biochar was presumably from the activator KOH. After adsorption, these peaks disappeared (Figure 6), which was mainly because of the ion exchange of K^+ and NH_4^+ during the adsorption process [48].

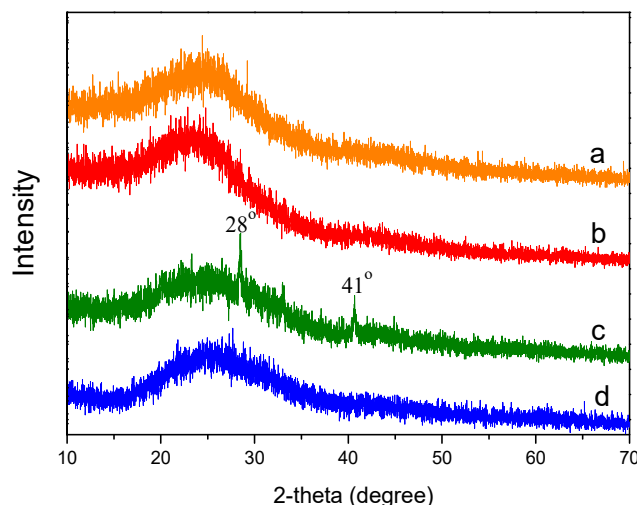


Figure 6. XRD patterns of NaOH-activated biochar before (a) and after (b) ammonium nitrogen adsorption and KOH-activated biochar before (c) and after (d) ammonium nitrogen adsorption.

3.3.3. Thermogravimetry (TG)

Figure 7 shows the thermogravimetric curves of SDG and NaOH-activated and KOH-activated biochars. The weight loss of SDG started when the temperature was increased to 200 °C, and over 60% weight loss was observed at the temperature of 500 °C, indicating that the SDG contained a large number of volatile substances [21]. However, no weight losses were observed for the two biochars until the temperature reached 350 °C, and their total weight losses (to 800 °C) were less than 25%, suggesting good thermal stability of the two prepared biochars. By contrasting the two biochars, it was found that the temperature at which the main weight loss started for NaOH-activated biochar was slightly higher than that for KOH-activated biochar. This result can presumably be attributed to the higher content of functional groups in the KOH-activated biochar (FTIR results), which tend to decompose during TG measurements.

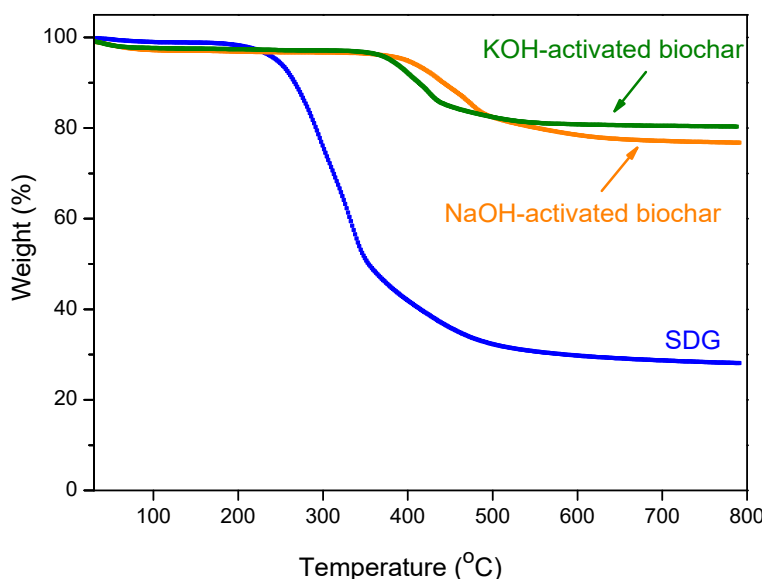


Figure 7. Thermogravimetric curves of sorghum distillers grain (SDG), NaOH-activated biochar, and KOH-activated biochar.

3.3.4. Fourier Transform Infrared Spectroscopy (FTIR)

The $\text{NH}_4^+ \text{-N}$ adsorption capacity of biochar depends not only on the specific surface area, but also on the contents of functional groups on its surface. The FTIR spectra of NaOH-activated and KOH-activated biochars are shown in Figure 8. Interestingly, NaOH-activated biochar exhibited a significantly different FTIR spectrum compared with the biochar activated by KOH. No obvious absorptions were found from the FTIR spectrum of NaOH-activated biochar in the range of $4000\text{--}400\text{ cm}^{-1}$, indicating the relative absence of functional groups on its surface. However, the KOH-activated biochars presented obviously enhanced absorption peak amount and intensity: a broad band at about 3420 cm^{-1} attributed to hydroxyl group stretching vibration [12,17], two bands at 1590 cm^{-1} and 1384 cm^{-1} assigned to the stretching vibration of asymmetric and symmetric COO^- of deprotonated carboxylate functional groups [49], and a 1045 cm^{-1} band caused by a $\text{C}-\text{O}-\text{C}$ stretching mode [17]. Thus, the FTIR results indicated that the KOH-activated biochar had much more functional groups, e.g., hydroxyl groups and carboxyl groups, which are critical for the adsorption of $\text{NH}_4^+ \text{-N}$ by electrostatic interaction [50]. Moreover, Boehm titrations were applied to analyze the oxygen-containing functional group contents of the two obtained biochars. The result showed that carboxyl and lactonic groups were present in KOH-activated biochar at 0.21 mmol/g and 0.08 mmol/g , respectively, much higher than the levels in NaOH-activated biochar (0.03 mmol/g and 0.02 mmol/g).

Physical and chemical adsorption are two main factors for effective $\text{NH}_4^+ \text{-N}$ adsorption by biochar [17]. The physical adsorption capacity depends mainly on the adsorbent porous structure, since the adsorbate is captured through nonselective Van der Waals forces [17]. Nevertheless, chemical adsorption relates to the properties of the adsorbate and the contents of functional groups on the adsorbent surface. Thus, for physical adsorption, the adsorption capacity relies primarily on the specific surface area of the adsorbent, which quantitatively represents the porous structure [21]. Here, the NaOH-activated biochar had higher specific surface area compared with the KOH-activated biochar but lower $\text{NH}_4^+ \text{-N}$ adsorption capacity, suggesting that physical adsorption is not the main factor in $\text{NH}_4^+ \text{-N}$ adsorption by the biochar. According to the FTIR results, KOH-activated biochar has a much higher content of functional groups compared with NaOH-activated biochar and, accordingly, has higher adsorption capacity. Therefore, chemical adsorption is the main reason for the better $\text{NH}_4^+ \text{-N}$ removal ability of KOH-activated biochar, which was also confirmed by the activation energy from the kinetics results.

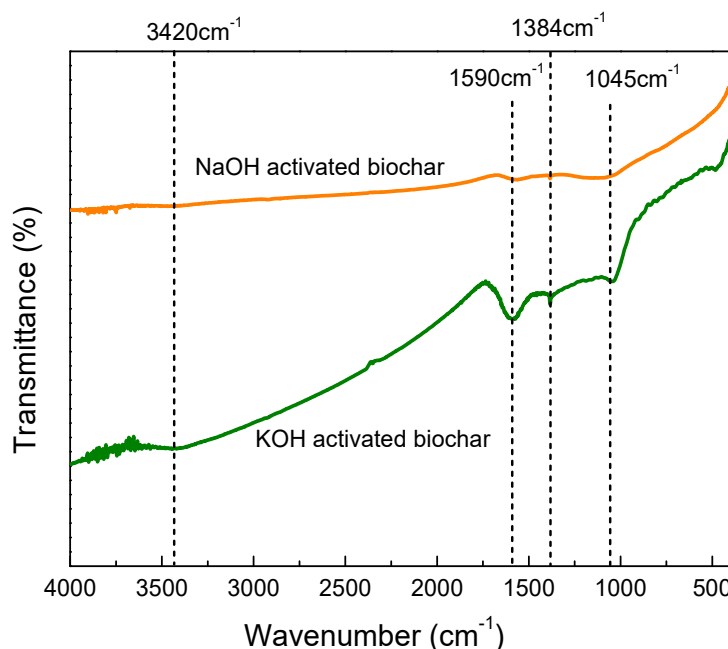


Figure 8. FTIR spectra of NaOH-activated biochar and KOH-activated biochar.

4. Conclusions

Two biochars from sorghum distillers grain were prepared through KOH and NaOH activation followed by pyrolysis for the first time. They both presented enhanced NH_4^+ -N adsorption capacity compared with the original biochar, owing to the significantly enhanced specific surface area after activation. The KOH-activated biochar had higher adsorption capacity than did the NaOH-activated biochar because of its much higher content of functional groups. The kinetics of NH_4^+ -N adsorption onto KOH-activated biochar followed a pseudo-second-order model, and the adsorption equilibrium data suggested that NH_4^+ -N adsorption fitted the Freundlich model well. The thermodynamic parameters demonstrated that the adsorption process was endothermic and spontaneous. The maximum adsorption capacity was found to be 14.34 mg/g at 45 °C, which was satisfactory when compared with other biochars prepared from different feedstocks. This work demonstrates that chemically activated biochar from sorghum distillers grain is a novel and efficient adsorbent for NH_4^+ -N removal.

Author Contributions: Conceptualization, D.H., C.L., and G.W.; methodology, D.H. and T.P., writing—original draft preparation, D.H. and T.P., writing—review and editing, D.H., C.L., Y.W., and G.W.

Funding: This research was funded by the National Natural Science Foundation of China (31700515).

Acknowledgments: This work was kindly supported by the National Natural Science Foundation of China (31700515).

Conflicts of Interest: The authors declare no conflict of interest.

References

1. Crini, G.; Lichtfouse, E. Advantages and disadvantages of techniques used for wastewater treatment. *Environ. Chem. Lett.* **2019**, *17*, 145–155. [[CrossRef](#)]
2. Cadar, O.; Miclean, M.; Cadar, S.; Tanaselia, C.; Senila, L.; Senila, M. Assessment of heavy metals in cows milk in Rodnei Mountains Area, Romania. *Environ. Eng. Manag. J.* **2015**, *14*, 2523–2528. [[CrossRef](#)]
3. Hoaghia, M.A.; Cadar, O.; Hognogi, G.G.; Levei, E.; Moisa, C.; Roman, C. Quality and Human Health Risk Assessment of Metals and Nitrogen Compounds in Drinking Water from an Urban Area Near a Former Non-Ferrous Ore Smelter. *Anal. Lett.* **2019**, *52*, 1268–1281. [[CrossRef](#)]

4. Moussavi, G.; Mahdavianpour, M. The selective direct oxidation of ammonium in the contaminated water to nitrogen gas using the chemical-less VUV photochemical continuous-flow reactor. *Chem. Eng. J.* **2016**, *295*, 57–63. [[CrossRef](#)]
5. Schindler, D.W.; Hecky, R.; Findlay, D.; Stainton, M.; Parker, B.; Paterson, M.; Beaty, K.; Lyng, M.; Kasian, S. Eutrophication of lakes cannot be controlled by reducing nitrogen input: Results of a 37-year whole-ecosystem experiment. *Proc. Natl. Acad. Sci. USA* **2008**, *105*, 11254–11258. [[CrossRef](#)]
6. Wang, Y.F.; Lin, F.; Pang, W.Q. Ammonium exchange in aqueous solution using Chinese natural clinoptilolite and modified zeolite. *J. Hazard. Mater.* **2007**, *142*, 160–164. [[CrossRef](#)]
7. Carrera, J.; Vicent, T.; Lafuente, J. Effect of influent COD/N ratio on biological nitrogen removal (BNR) from high-strength ammonium industrial wastewater. *Process Biochem.* **2004**, *39*, 2035–2041. [[CrossRef](#)]
8. Thornton, A.; Pearce, P.; Parsons, S. Ammonium removal from digested sludge liquors using ion exchange. *Water Res.* **2007**, *41*, 433–439. [[CrossRef](#)]
9. Kizito, S.; Wu, S.; Kirui, W.K.; Lei, M.; Lu, Q.; Bah, H.; Dong, R. Evaluation of slow pyrolyzed wood and rice husks biochar for adsorption of ammonium nitrogen from piggery manure anaerobic digestate slurry. *Sci. Total Environ.* **2015**, *505*, 102–112. [[CrossRef](#)]
10. Shah, T.M.; Ramaswami, S.; Behrendt, J.; Otterpohl, R. Simultaneous removal of organics and ammonium-nitrogen from reverse osmosis concentrate of mature landfill leachate. *J. Water Process Eng.* **2017**, *19*, 126–132. [[CrossRef](#)]
11. Mook, W.T.; Chakrabarti, M.H.; Aroua, M.K.; Khan, G.M.A.; Ali, B.S.; Islam, M.S.; Abu Hassan, M.A. Removal of total ammonia nitrogen (TAN), nitrate and total organic carbon (TOC) from aquaculture wastewater using electrochemical technology: A review. *Desalination* **2012**, *285*, 1–13. [[CrossRef](#)]
12. Yu, Q.; Dong, X.; Li, H.; Ke, L.; Wang, Y.; Wang, H.; Zheng, Y.; Li, Q. Effectiveness and mechanisms of ammonium adsorption on Biochars derived from biogas residues. *RSC Adv.* **2016**, *6*, 88373–88381. [[CrossRef](#)]
13. Wang, G.; Liu, Q.; Chang, M.; Jang, J.; Sui, W.; Si, C.; Ni, Y. Novel Fe₃O₄@lignosulfonate/phenolic core-shell microspheres for highly efficient removal of cationic dyes from aqueous solution. *Ind. Crops Prod.* **2019**, *127*, 110–118. [[CrossRef](#)]
14. Liu, J.; Su, Y.; Li, Q.; Yue, Q.; Gao, B. Preparation of wheat straw based superabsorbent resins and their applications as adsorbents for ammonium and phosphate removal. *Bioresour. Technol.* **2013**, *143*, 32–39. [[CrossRef](#)] [[PubMed](#)]
15. Zheng, Y.; Xie, Y.; Wang, A. Rapid and wide pH-independent ammonium-nitrogen removal using a composite hydrogel with three-dimensional networks. *Chem. Eng. J.* **2012**, *179*, 90–98. [[CrossRef](#)]
16. Ahmad, M.; Rajapaksha, A.U.; Lim, J.E.; Zhang, M.; Bolan, N.; Mohan, D.; Vithanage, M.; Lee, S.S.; Ok, Y.S. Biochar as a sorbent for contaminant management in soil and water: A review. *Chemosphere* **2014**, *99*, 19–33. [[CrossRef](#)]
17. Zhang, J.; Wang, Q. Sustainable mechanisms of biochar derived from brewers' spent grain and sewage sludge for ammonia–nitrogen capture. *J. Clean. Prod.* **2016**, *112*, 3927–3934. [[CrossRef](#)]
18. Zhao, Y.; Yang, Y.; Yang, S.; Wang, Q.; Feng, C.; Zhang, Z. Adsorption of high ammonium nitrogen from wastewater using a novel ceramic adsorbent and the evaluation of the ammonium-adsorbed-ceramic as fertilizer. *J. Colloid Interface Sci.* **2013**, *393*, 264–270. [[CrossRef](#)]
19. Su, M.Y.; Tzeng, W.S.; Shyu, Y.T. An analysis of feasibility of bioethanol production from Taiwan sorghum liquor waste. *Bioresour. Technol.* **2010**, *101*, 6669–6675. [[CrossRef](#)]
20. Zheng, X.; Yang, Z.; Xu, X.; Dai, M.; Guo, R. Characterization and ammonia adsorption of biochar prepared from distillers' grains anaerobic digestion residue with different pyrolysis temperatures. *J. Chem. Technol. Biotechnol.* **2018**, *93*, 198–206. [[CrossRef](#)]
21. Xia, D.; Tan, F.; Zhang, C.; Jiang, X.; Chen, Z.; Li, H.; Zheng, Y.; Li, Q.; Wang, Y. ZnCl₂-activated biochar from biogas residue facilitates aqueous As (III) removal. *Appl. Surf. Sci.* **2016**, *377*, 361–369. [[CrossRef](#)]
22. Zhu, Y.; Kolar, P.; Shah, S.B.; Cheng, J.J.; Lim, P.K. Avocado seed-derived activated carbon for mitigation of aqueous ammonium. *Ind. Crops Prod.* **2016**, *92*, 34–41. [[CrossRef](#)]
23. Yusof, A.M.; Keat, L.K.; Ibrahim, Z.; Majid, Z.A.; Nizam, N.A. Kinetic and equilibrium studies of the removal of ammonium ions from aqueous solution by rice husk ash-synthesized zeolite Y and powdered and granulated forms of mordenite. *J. Hazard. Mater.* **2010**, *174*, 380–385. [[CrossRef](#)] [[PubMed](#)]

24. Ciftci, O.N.; Calderon, J.; Temelli, F. Supercritical carbon dioxide extraction of corn distiller's dried grains with solubles: Experiments and mathematical modeling. *J. Agric. Food Chem.* **2012**, *60*, 12482–12490. [CrossRef] [PubMed]
25. Miller, G.L. Use of dinitrosalicylic acid reagent for determination of reducing sugar. *Anal. Chem.* **1959**, *31*, 426–428. [CrossRef]
26. Yang, Y.; Wei, Z.; Zhang, X.; Chen, X.; Yue, D.; Yin, Q.; Xiao, L.; Yang, L. Biochar from Alternanthera philoxeroides could remove Pb(II) efficiently. *Bioresour. Technol.* **2014**, *171*, 227–232. [CrossRef] [PubMed]
27. Li, H.; Jiao, A.; Wei, B.; Wang, Y.; Wu, C.; Jin, Z.; Tian, Y. Porous starch extracted from Chinese rice wine vinasse: Characterization and adsorption properties. *Int. J. Biol. Macromol.* **2013**, *61*, 156–159. [CrossRef]
28. Gai, X.; Wang, H.; Liu, J.; Zhai, L.; Liu, S.; Ren, T.; Liu, H. Effects of Feedstock and Pyrolysis Temperature on Biochar Adsorption of Ammonium and Nitrate. *PLoS ONE* **2014**, *9*, e113888. [CrossRef]
29. Azargohar, R.; Dalai, A.K. Steam and KOH activation of biochar: Experimental and modeling studies. *Microporous Mesoporous Mater.* **2008**, *110*, 413–421. [CrossRef]
30. Ahmad, M.; Lee, S.S.; Rajapaksha, A.U.; Vithanage, M.; Zhang, M.; Cho, J.S.; Lee, S.E.; Ok, Y.S. Trichloroethylene adsorption by pine needle biochars produced at various pyrolysis temperatures. *Bioresour. Technol.* **2013**, *143*, 615–622. [CrossRef]
31. Brown, R.A.; Kercher, A.K.; Nguyen, T.H.; Nagle, D.C.; Ball, W.P. Production and characterization of synthetic wood chars for use as surrogates for natural sorbents. *Org. Geochem.* **2006**, *37*, 321–333. [CrossRef]
32. Jing, Q.X.; Chai, L.Y.; Huang, X.D.; Tang, C.J.; Guo, H.; Wang, W. Behavior of ammonium adsorption by clay mineral halloysite. *Trans. Nonferrous Met. Soc. China* **2017**, *27*, 1627–1635. [CrossRef]
33. Vu, T.M.; Trinh, V.T.; Doan, D.P.; Van, H.T.; Nguyen, T.V.; Vigneswaran, S.; Ngo, H.H. Removing ammonium from water using modified corncob-biochar. *Sci. Total Environ.* **2017**, *579*, 612–619. [CrossRef] [PubMed]
34. Wang, B.; Lehmann, J.; Hanley, K.; Hestrin, R.; Enders, A. Adsorption and desorption of ammonium by maple wood biochar as a function of oxidation and pH. *Chemosphere* **2015**, *138*, 120–126. [CrossRef] [PubMed]
35. Ferreira, B.C.S.; Teodoro, F.S.; Mageste, A.B.; Gil, L.F.; de Freitas, R.P.; Gurgel, L.V.A. Application of a new carboxylate-functionalized sugarcane bagasse for adsorptive removal of crystal violet from aqueous solution: Kinetic, equilibrium and thermodynamic studies. *Ind. Crops Prod.* **2015**, *65*, 521–534. [CrossRef]
36. Hu, J.; Lo, I.M.; Chen, G. Fast removal and recovery of Cr (VI) using surface-modified jacobsite (MnFe_2O_4) nanoparticles. *Langmuir* **2005**, *21*, 11173–11179. [CrossRef]
37. Zhang, J.; Lin, X.; Luo, X.; Zhang, C.; Zhu, H. A modified lignin adsorbent for the removal of 2, 4, 6-trinitrotoluene. *Chem. Eng. J.* **2011**, *168*, 1055–1063. [CrossRef]
38. Başar, C.A. Applicability of the various adsorption models of three dyes adsorption onto activated carbon prepared waste apricot. *J. Hazard. Mater.* **2006**, *135*, 232–241. [CrossRef]
39. Tseng, R.L.; Wu, F.C. Inferring the favorable adsorption level and the concurrent multi-stage process with the Freundlich constant. *J. Hazard. Mater.* **2008**, *155*, 277–287. [CrossRef]
40. Huang, X.; Gao, N.Y.; Zhang, Q.L. Thermodynamics and kinetics of cadmium adsorption onto oxidized granular activated carbon. *J. Environ. Sci.* **2007**, *19*, 1287–1292. [CrossRef]
41. Fu, J.; Chen, Z.; Wang, M.; Liu, S.; Zhang, J.; Zhang, J.; Han, R.; Xu, Q. Adsorption of methylene blue by a high-efficiency adsorbent (polydopamine microspheres): Kinetics, isotherm, thermodynamics and mechanism analysis. *Chem. Eng. J.* **2015**, *259*, 53–61. [CrossRef]
42. Bulut, Y.; Aydin, H. A kinetics and thermodynamics study of methylene blue adsorption on wheat shells. *Desalination* **2006**, *194*, 259–267. [CrossRef]
43. Sadraei, R.; Paganini, C.M.; Calza, P.; Magnacca, G. An Easy Synthesis for Preparing Bio-Based Hybrid Adsorbent Useful for Fast Adsorption of Polar Pollutants. *Nanomaterials* **2019**, *9*, 731. [CrossRef] [PubMed]
44. Sadraei, R.; Murphy, R.S.; Laurenti, E.; Magnacca, G. Characterization Methodology To Evaluate the Activity of Supported Soybean Peroxidase. *Ind. Eng. Chem. Res.* **2019**, *58*, 19082–19089. [CrossRef]
45. Bansode, R.R.; Losso, J.N.; Marshall, W.E.; Rao, R.M.; Portier, R.J. Pecan shell-based granular activated carbon for treatment of chemical oxygen demand (COD) in municipal wastewater. *Bioresour. Technol.* **2004**, *94*, 129–135. [CrossRef]
46. Tang, Y.B.; Liu, Q.; Chen, F.Y. Preparation and characterization of activated carbon from waste ramulus mori. *Chem. Eng. J.* **2012**, *203*, 19–24. [CrossRef]

47. Feng, Y.; Zhou, H.; Liu, G.; Qiao, J.; Wang, J.; Lu, H.; Yang, L.; Wu, Y. Methylene blue adsorption onto swede rape straw (*Brassica napus* L.) modified by tartaric acid: Equilibrium, kinetic and adsorption mechanisms. *Bioresour. Technol.* **2012**, *125*, 138–144. [[CrossRef](#)]
48. Mukherjee, A.; Zimmerman, A.; Harris, W. Surface chemistry variations among a series of laboratory-produced biochars. *Geoderma* **2011**, *163*, 247–255. [[CrossRef](#)]
49. Wahab, M.A.; Jellali, S.; Jedidi, N. Ammonium biosorption onto sawdust: FTIR analysis, kinetics and adsorption isotherms modeling. *Bioresour. Technol.* **2010**, *101*, 5070–5075. [[CrossRef](#)]
50. Li, R.; Wang, J.J.; Zhou, B.; Zhang, Z.; Liu, S.; Lei, S.; Xiao, R. Simultaneous capture removal of phosphate, ammonium and organic substances by MgO impregnated biochar and its potential use in swine wastewater treatment. *J. Clean. Prod.* **2017**, *147*, 96–107. [[CrossRef](#)]



© 2019 by the authors. Licensee MDPI, Basel, Switzerland. This article is an open access article distributed under the terms and conditions of the Creative Commons Attribution (CC BY) license (<http://creativecommons.org/licenses/by/4.0/>).